J Freezing and Hund's Rules in Spin-Orbit-Coupled Multiorbital Hubbard Models

Aaram J. Kim,[1,*] Harald O. Jeschke,[1] Philipp Werner,[2] and Roser Valentí[1]
[1]Institut für Theoretische Physik, Goethe-Universität Frankfurt, Max-von-Laue-Straße 1, 60438 Frankfurt am Main, Germany
[2]Department of Physics, University of Fribourg, Chemin du Musée 3, 1700 Fribourg, Switzerland
(Received 18 July 2016; published 21 February 2017)

We investigate the phase diagram of the spin-orbit-coupled three orbital Hubbard model at arbitrary filling by means of dynamical mean-field theory combined with the continuous-time quantum Monte Carlo method. We find that the spin-freezing crossover occurring in the metallic phase of the nonrelativistic multiorbital Hubbard model can be generalized to a **J**-freezing crossover, with $\mathbf{J} = \mathbf{L} + \mathbf{S}$, in the spin-orbit-coupled case. In the **J**-frozen regime the correlated electrons exhibit a nontrivial flavor selectivity and energy dependence. Furthermore, in the regions near $n = 2$ and $n = 4$ the metallic states are qualitatively different from each other, which reflects the atomic Hund's third rule. Finally, we explore the appearance of magnetic order from exciton condensation at $n = 4$ and discuss the relevance of our results for real materials.

DOI: 10.1103/PhysRevLett.118.086401

Introduction.—In $4d$ and $5d$ transition metal oxides the interplay and competition between kinetic energy, spin-orbit coupling (SOC), and correlation effects results in several interesting phenomena, such as spin-orbit assisted Mott transitions [1–6], unconventional superconductivity [7,8], topological phases [9], exciton condensation [8,10,11], or exotic magnetic orders [12,13]. Transition metal oxides involving $4d$ and $5d$ electrons show diverse structures like the Ruddlesden-Popper series [1,7], double perovskite, [12–14] two-dimensional honeycomb geometry [3–6,15,16] or pyrochlore lattices [17]. In an octahedral environment, as in most of the $4d$ and $5d$ materials mentioned above, the five d orbitals are split into low energy t_{2g} and higher energy e_g levels. The SOC further splits the low energy t_{2g} levels into a so-called $j = 1/2$ doublet and $j = 3/2$ quadruplet. The energy separation between the $j = 1/2$ and $j = 3/2$ bands is proportional to the strength of the SOC. Existing *ab initio* density functional theory calculations [17,18] suggest that in some materials a multiorbital description including both the $j = 1/2$ and $j = 3/2$ subbands should be considered.

Most theoretical studies of $4d$ and $5d$ systems have focused on material-specific models with fixed electronic filling. Here we follow a different strategy and explore the possible states that emerge from a multiband Hubbard model with spin-orbit coupling at arbitrary filling. This allows us to investigate unexplored regions in parameter space which may exhibit interesting phenomena. Specifically, by performing a systematic analysis of the local **J** moment susceptibility ($\mathbf{J} = \mathbf{L} + \mathbf{S}$) as a function of Coulomb repulsion U, Hund's coupling J_H, spin-orbit coupling λ, and filling n, we identify Mott-Hubbard insulating phases and complex metallic states. We find a **J**-freezing crossover between a Fermi liquid (FL) and a non-Fermi liquid (NFL) phase where the latter shows a distinct flavor selectivity that originates from the SOC. In addition, we observe a strong asymmetry in the metallic phase between filling $n = 2$ and $n = 4$ with properties reminiscent of the atomic Hund's third rule. Finally, we investigate doping effects on the excitonic magnetism at $n = 4$.

Method.—We consider a three-orbital Hubbard model with spin-orbit coupling. The model Hamiltonian consists of three terms,

$$\mathcal{H} = \mathcal{H}_t + \mathcal{H}_\lambda + \mathcal{H}_U, \tag{1}$$

where $\mathcal{H}_t$, $\mathcal{H}_\lambda$, and $\mathcal{H}_U$ denote the electron hopping, spin-orbit coupling, and local Coulomb interaction terms, respectively. In order to discuss the underlying physics, relevant for a range of materials with different structures, we use a semicircular density of states (DOS), $\rho^0(\omega) = (2/\pi D)\sqrt{1-(\omega/D)^2}$ for all orbitals. The half bandwidth D is set to unity. $\mathcal{H}_\lambda$ is constructed by projecting the SOC term of d orbitals onto the t_{2g} subspace,

$$\mathcal{H}_\lambda = \lambda \sum_{\substack{\alpha\beta \\ \sigma\sigma'}} c^\dagger_{i\alpha\sigma} \langle \alpha\sigma | \mathcal{P}_{t_{2g}} \mathbf{L}^d \mathcal{P}_{t_{2g}} \cdot \mathbf{S} | \beta\sigma' \rangle c_{i\beta\sigma'}, \tag{2}$$

where $\mathcal{P}_{t_{2g}}$ is the projection operator. $c_{i\alpha\sigma}$ ($c^\dagger_{i\alpha\sigma}$) denotes the annihilation (creation) operator of a spin σ electron at site i and orbital α. The angular momentum operator within the t_{2g} subspace can be represented by an effective $L = 1$ angular momentum operator with an extra minus sign [12].

The local Coulomb interaction Hamiltonian is written in Kanamori form [19] including the spin-flip and pair-hopping terms as

$$\begin{aligned}\mathcal{H}_U = {} & U \sum_{i,\alpha} n_{i\alpha\uparrow} n_{i\alpha\downarrow} + \sum_{\substack{i,\alpha<\alpha' \\ \sigma\sigma'}} (U' - J_H \delta_{\sigma\sigma'}) n_{i\alpha\sigma} n_{i\alpha'\sigma'} \\ & - J_H \sum_{i,\alpha<\alpha'} (c^\dagger_{i\alpha\uparrow} c^\dagger_{i\alpha'\downarrow} c_{i\alpha'\uparrow} c_{i\alpha\downarrow} + \text{H.c.}) \\ & + J_H \sum_{i,\alpha<\alpha'} (c^\dagger_{i\alpha\uparrow} c^\dagger_{i\alpha\downarrow} c_{i\alpha'\downarrow} c_{i\alpha'\uparrow} + \text{H.c.}).\end{aligned} \tag{3}$$

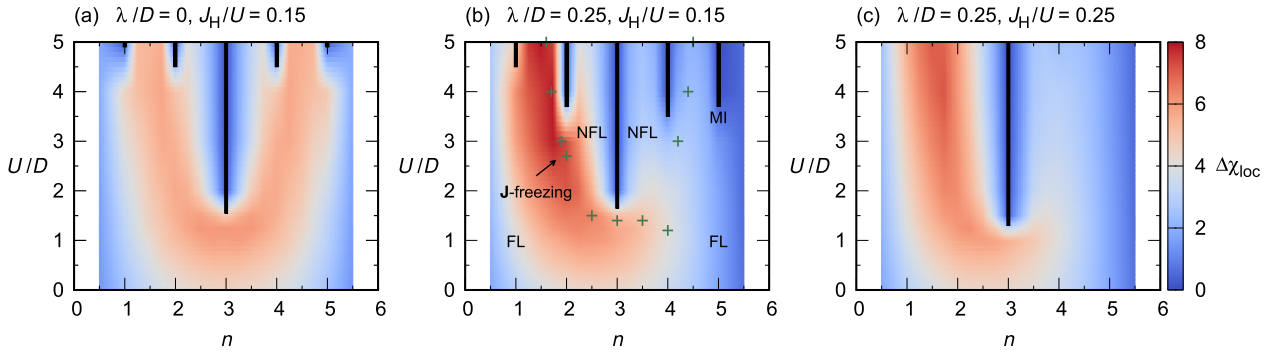

FIG. 1. Dynamic contribution to the local susceptibility, $\Delta\chi_{\mathrm{loc}}$ in the $(U/D, n)$ phase diagram for (a) $\lambda/D = 0.0$, $J_H/U = 0.15$, (b) $\lambda/D = 0.25$, $J_H/U = 0.15$, (c) $\lambda/D = 0.25$, $J_H/U = 0.25$, and $T/D = 0.03$. Cross symbols mark the maximum values of $\Delta\chi_{\mathrm{loc}}$ corresponding to the **J**-freezing crossover points. The parameter set for (b) corresponds roughly to the tight-binding parameters for Sr_2IrO_4 [32]. The reported values of λ, J_H, and U for various materials are summarized in the Supplemental Material [25].

Here, U is the on-site Coulomb interaction and J_H denotes the Hund's coupling. U' is set to $U - 2J_H$ to make the interaction rotationally invariant in orbital space.

We employ the dynamical mean-field theory (DMFT) [20] to solve the model Hamiltonian Eq. (1) in a broad parameter space. Since DMFT is a nonperturbative technique within the local self-energy approximation, we can access metallic and insulating phases on the same footing. In addition, the dynamical fluctuations encoded in the DMFT solution contain valuable information on the degree of moment correlations and the corresponding susceptibility. We will use the local **J** moment susceptibility as a central quantity to investigate the phase diagram.

As an impurity solver, we adopt the continuous-time quantum Monte Carlo method (CTQMC) in the hybridization expansion variant [21,22]. For the single particle basis of the CTQMC calculation, we choose the relativistic j effective basis ($j = 1/2$, $j = 3/2$) which is an eigenbasis of the SOC Hamiltonian. It was previously reported that the j effective basis reduces the sign problem of the CTQMC simulation [23]. For symmetry broken phases, we consider the off-diagonal hybridization functions.

Results.—A strong Coulomb interaction localizes electrons and can lead to the formation of local moments. The freezing of these local moments is signaled by a slow decay, and eventual saturation, of the dynamical correlation function $\langle J_z(\tau)J_z(0)\rangle$ on the imaginary-time axis. Hence, the local susceptibility, defined as

$$\chi_{\mathrm{loc}} = \int_0^\beta d\tau \langle J_z(\tau)J_z(0)\rangle, \tag{4}$$

allows us to investigate the formation and freezing of local moments. In addition, we define the dynamical contribution to the local susceptibility by eliminating the long-term memory of the correlation function from the original χ_{loc} [24]:

$$\Delta\chi_{\mathrm{loc}} = \int_0^\beta d\tau (\langle J_z(\tau)J_z(0)\rangle - \langle J_z(\beta/2)J_z(0)\rangle). \tag{5}$$

As the system evolves from an itinerant to a localized phase, $\Delta\chi_{\mathrm{loc}}$ exhibits a maximum in the intermediate Coulomb interaction regime [see Figs. S1(c), S1(d) in the Supplemental Material [25]]; both, (i) the enhanced correlations compared to the noninteracting limit and (ii) the larger fluctuations compared to the localized limit lead to the maximum in $\Delta\chi_{\mathrm{loc}}$. The location of the $\Delta\chi_{\mathrm{loc}}$ maxima in the phase diagram can be viewed as the boundary of the local moment regime and has been used to define the spin-freezing crossover line in the non-spin-orbit coupled system [24,33]. However, since spin is not a good quantum number in the spin-orbit-coupled system, we introduce the total moment $\mathbf{J} = \mathbf{S} + \mathbf{L}$ to generalize the "spin-freezing" to a "**J**-freezing" crossover.

In the following, we discuss the paramagnetic phase diagram of Eq. (1) obtained with DMFT(CTQMC) as a function of U, J_H, λ, and n. Figures 1(a)–1(c) show contour plots of $\Delta\chi_{\mathrm{loc}}$ in the interaction vs the filling plane for three different parameter sets of λ and J_H. Since SOC breaks particle-hole symmetry, Figs. 1(b),1(c) are not symmetric about the half-filling axis, $n = 3$. The Mott insulating phase (black lines in Fig. 1) which we identify as the region where the spectral function vanishes at the Fermi level and where $\Delta\chi_{\mathrm{loc}}$ is smallest, appears at each commensurate filling. Nonetheless, compared to the system without SOC [Fig. 1(a)], the change of the critical interaction strength U_c shows a complex behavior depending on the filling and λ. We can quantitatively analyze the change of U_c using the Mott-Hubbard criterion, according to which a Mott transition occurs when the atomic charge gap becomes comparable to the average kinetic energy:

$$\Delta_{\mathrm{ch}}(n, U_c, J_H, \lambda) \equiv U_c + \delta\Delta_{\mathrm{ch}}(n, J_H, \lambda) = \tilde{W}(n, J_H, \lambda). \tag{6}$$

Δ_{ch} is the charge gap of the local Hamiltonian, and $\tilde{W}(n, J_H, \lambda)$ is the average kinetic energy. Here, n is integer for commensurate Mott insulators. Since SOC reduces the degeneracy of the atomic ground states, $\tilde{W}$ is basically a

decreasing function of λ except for $n = 3$, where the ground state degeneracy is not changed by introducing SOC. By diagonalizing the local Hamiltonian, we observe that $\delta\Delta_{\rm ch}$ is an increasing function of λ for $n = 1$, 2, and 4, but a decreasing function for $n = 3$ and 5. Altogether, for $n = 1$, 2, and 4, the two terms contributing to $U_c = \tilde{W} - \delta\Delta_{\rm ch}$ cooperate to reduce U_c as we also observe in our DMFT results. A smaller U_c at $n = 4$ compared to $n = 2$ is consistent with the Mott-Hubbard criterion. In contrast, for $n = 5$ the two contributions to U_c compete and it is hard to predict the behavior of U_c from this criterion. We can anticipate based on the DMFT results that the reduction of the kinetic energy dominates the slight decrease of the atomic gap. Finally, at $n = 3$ there is an unchanged degeneracy and $\delta\Delta_{\rm ch}$ decreases due to SOC implying a slight increase of U_c [compare Fig. 1(a) and 1(b) and see Fig. S4 in Ref. [25]].

The effect of the Hund's coupling can be seen by comparing Figs. 1(b) and 1(c). Away from half-filling, U_c increases with J_H but at half-filling it slightly decreases, which is consistent with the behavior of $\delta\Delta_{\rm ch}$ [34]. For even stronger SOC, $\lambda/D = 0.5$, a drastically reduced U_c is found at $n = 4$ implying an adiabatic connection of the Mott insulator to the band insulator in the $\lambda \gg 1$ limit [25,35].

We now concentrate on the metallic regions. In the spin-orbit-coupled multiorbital system the dynamic contribution to the susceptibility is larger below half-filling compared to the particle-hole transformed state [red area in Fig. 1(b) and 1(c)]. Such a difference mainly comes from the cross-correlation between the spin and the orbital moment, which is positive for $n < 3$ and negative for $n > 3$ [see Fig. S3(d) in Ref. [25]]. A recent study [24] has shown that in the case of a multiorbital Hubbard model without spin-orbit coupling, s-wave spin-triplet superconductivity can appear along the spin-freezing line. The effect of the spin-orbital cross-correlation on this superconductivity will be an interesting future research topic.

The asymmetry in the susceptibility and dynamical contribution to the susceptibility below and above half-filling can be explained by Hund's third rule whose origin is the spin-orbit coupling [25,36,37]. Following Hund's third rule, in the atomic limit the alignment between **L** and **S** depends on whether the filling is below or above half-filling. In our calculation, **L** and **S** are aligned in the same direction below half-filling, while they are antialigned above half-filling. Therefore, the size of the total **J**-moment is larger at fillings below $n = 3$ as we increase the interaction strength and further localize the electrons. Figure 2 shows the evolution of $\langle J_z^2 \rangle$ as a function of Coulomb interaction strength for five commensurate fillings and parameter values as chosen in Fig. 1(b). In the intermediate and strong interaction region, $U/D \gtrsim 2$, an enhanced value of the **J**-moment is found at $n = 2$ and 1 compared to the cases $n = 4$ and 5, respectively. In the strong correlation (Mott insulating) regime, the alignment of the spin, orbital, and **J**-moment is consistent

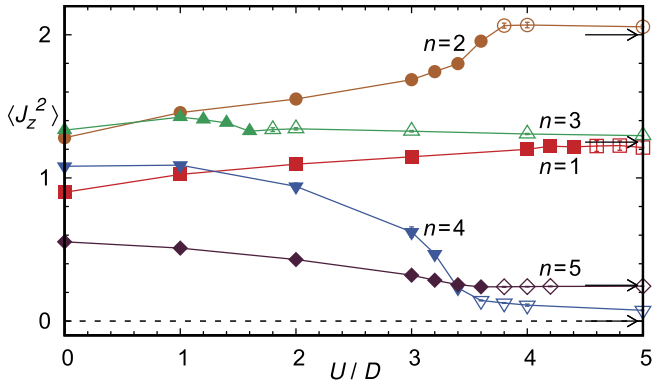

FIG. 2. Size of the local J_z moments as a function of interaction strength U/D for $\lambda/D = 0.25$, $J_H/U = 0.15$, and $T/D = 0.03$ at various commensurate fillings. The parameter set is the same as in Fig. 1(b). Solid (open) symbols correspond to the metallic (insulating) solutions. The arrows represent the corresponding values from the Hund's rule.

with the atomic results according to Hund's rules. The **J**-moment determined by the atomic Hund's rule has a strong effect on the $\Delta\chi_{\rm loc}$ and $\chi_{\rm loc}$ in the metallic phase even at moderate U values.

Inside the **J**-freezing region [denoted by crosses in Fig. 1(b)], we observe a non-Fermi liquid behavior of the metallic state. In order to explore this state we show in Figs. 3(a) and 3(b) the imaginary part of the self-energy on the Matsubara frequency axis across the **J**-freezing cross-over line for the same parameter values as in Fig. 1(b) and various fillings. In the low frequency region, $\mathrm{Im}\Sigma(i\omega_n)$ can be expressed in the form $-\Gamma - C\omega_n^{\alpha}$. As we cross the **J**-freezing line, (region between $n \simeq 2$ and $n \simeq 4$ for $U = 3$) Γ changes from zero to a finite value, indicating a Fermi-liquid to NFL crossover. Near the **J**-freezing line, a small Γ value with a noninteger exponent α is found.

These two characteristic properties of the FL to NFL crossover are reminiscent of the spin-freezing crossover observed in the model without SOC [33]. As the system gets closer to $n = 3$, the correlation function $\langle S_z(\tau)S_z(0)\rangle$ increases while that of $\langle L_z(\tau)L_z(0)\rangle$ and $\langle L_z(\tau)S_z(0)\rangle$ decreases in magnitude [25], so that the orbitally averaged scattering rate is determined primarily by the frozen spin moments. However, due to SOC, the self-energy $\mathrm{Im}\Sigma(i\omega_n)$ of the $j = 1/2$ electron is different from that of the $j = 3/2$ electrons. At low frequency, the difference between $j = 1/2$ and $3/2$ is enhanced in the NFL phase compared to the FL phase.

A remarkable finding is that there exists an intersection between the two self-energies from the different j bands in the NFL phase [see shadings in Figs. 3(a) and 3(b)]. This intersection implies that the scattering rate near the Fermi-level $\mathrm{Im}\Sigma(\omega \sim 0)$ and the total scattering rate $\int_{-\infty}^{\infty} d\omega\, \mathrm{Im}\Sigma(\omega)$ have different relative magnitudes for the $j = 1/2$ and $3/2$ electrons. For example, for $n = 3.5$, the $j = 3/2$ electrons have a larger value of Γ with larger

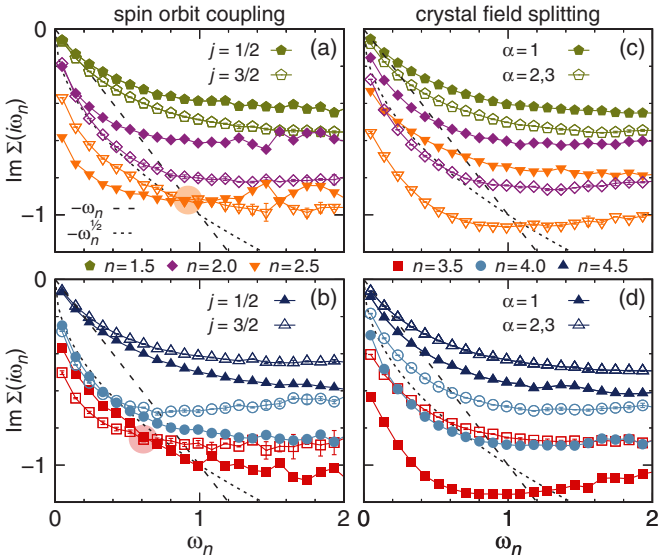

FIG. 3. Imaginary part of the self-energy on the Matsubara axis for the system with (a),(b) spin-orbit coupling (SOC) (c),(d) crystal-field (CF) splitting. For (c),(d) the CF Hamiltonian, $\mathcal{H}_{\mathrm{CF}} = \Delta_{\mathrm{CF}} \sum_{\sigma} n_{1\sigma}$ is introduced instead of $\mathcal{H}_{\mathrm{SOC}}$. The strength of the SOC and the CF are chosen to produce the same noninteracting DOS: $\lambda/D = 0.25$ and $\Delta_{\mathrm{CF}}/D = 0.375$. $U/D = 3.0$, $J_H/U = 0.15$, and $T/D = 0.015$. Solid (open) symbols in (a),(b) denote the $j = 1/2$ (3/2) results. Solid (open) symbols in (c),(d) correspond to $\alpha = 1$ ($\alpha = 2, 3$). For $j = 3/2$ in (a),(b) the average over $m_j = \pm 1/2, \pm 3/2$ is shown. In (c),(d), we plot the average of $\alpha = 2, 3$ and spin. The shadings in (a),(b) highlight the intersections between the different self-energies. The dashed (dotted) lines correspond to $-\omega_n$ ($-\omega_n^{0.5}$) as a guide for the low frequency scaling.

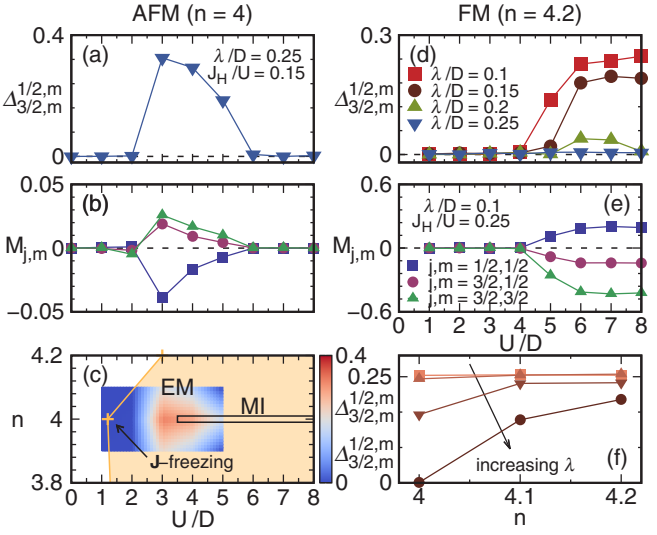

FIG. 4. (a) Excitonic order parameter and (b) magnetic components as a function of U/D at $T/D = 0.33$ for $n = 4.0$, $\lambda/D = 0.25$, and $J_H/U = 0.15$. (c) Density plot for the AFM excitonic order parameter. Here, EM represents the excitonic magnetism. The black bar and yellow line indicate the boundary of the (paramagnetic) metal-insulator (MI) and **J**-freezing regime, respectively. (d) Excitonic order parameter and (e) magnetic components as a function of U/D at $T/D = 0.33$ for $n = 4.2$, $J_H/U = 0.25$, and various λ/D values. (f) Doping dependence of the excitonic order parameter: from top to bottom, the corresponding λ/D values are 0.0, 0.05, 0.1, and 0.15, respectively.

scattering rate at the Fermi level, while they exhibit a smaller high energy coefficient of the $1/(i\omega_n)$ tail, implying a smaller total scattering rate. Such a behavior is not observed in the Hubbard model with ordinary crystal field (CF) splitting (no SOC) as shown in Figs. 3(c) and 3(d) [38]. We suggest that the basis transformation and corresponding modification of the interaction, especially of the Hund's coupling, are the origin of this phenomenon. This implies that the interplay between spin-orbit coupling effects and electronic correlation cannot be fully captured by an effective crystal-field splitting description. We call this phenomenon spin-orbit-correlation induced flavor selectivity.

Note that the frozen **J**-moment and the NFL behavior are characteristic features of multiorbital systems with large composite moments. Within the **J**-freezing region, even the $j = 1/2$ electrons show NFL behavior, and the single-band description for $j = 1/2$ is not valid anymore. Accordingly, the **J**-freezing crossover line delimits the region of validity of the single-band description.

Besides the paramagnetic phase, we also investigate the excitonic magnetism (EM) near $n = 4$ [8,10,11,39]. To access such a symmetry broken phase, we introduce the off-diagonal components of the Green function and define the order parameter of the exciton condensed phase as $\Delta_{jm}^{j'm'} = \langle c_{jm}^{\dagger} c_{j'm'} \rangle$, where $j' \neq j$. The magnetic components are defined as $M_{j,m} = \langle n_{j,+m} \rangle - \langle n_{j,-m} \rangle$. We find two types of magnetism: antiferromagnetism (AFM) and ferromagnetism (FM) at different fillings. At $n = 4$ an AFM excitonic state appears at intermediate interaction strength [8,39–42]. The corresponding region is located around the metal-insulator transition point of the paramagnetic calculations, $U_c/D \sim 3.5$. Figures 4(a) and 4(b) show that AFM ($M_{j,m} \neq 0$) and excitonic order ($\Delta_{3/2,m}^{1/2,m} \neq 0$) appear simultaneously. Upon electron doping, the AFM state is rapidly suppressed and eventually vanishes around $n \sim 4.2$, which is shown in Fig. 4(c).

Ba_2YIrO_6 is a d^4 system whose ground state is experimentally not completely resolved [43,44]. According to the realistic parameter values in Ba_2YIrO_6 as given in Table SV in the Supplemental Material (Ref. [25]), we would find a $J = 0$ state in this system.

For large Hund's coupling and small SOC, a FM state emerges in the strong interaction region [Figs. 4(d) and 4(e)]. However, the SOC effectively suppresses the FM state and drives the system into an AFM state at $n = 4$ (see Fig. S5 in Ref. [25]). Compared to the $n = 4$ case, the doped FM state at $n = 4.2$ is less sensitive to the SOC [Fig. 4(f)]. We expect that the larger kinetic energy gain for $n > 4$ favors the FM state.

Conclusions.—We have explored the paramagnetic phase diagram of the spin-orbit-coupled three-orbital Hubbard model at general filling. We found a generalized **J**-freezing crossover as a function of U, J_H, λ and n which exhibits a strong particle-hole asymmetry and we have detected a metallic phase with a large $\Delta\chi_{\mathrm{loc}}$ near $n = 2$ and a small $\Delta\chi_{\mathrm{loc}}$ near $n = 4$, which is the effect of Hund's third rule on the itinerant phase. Across the **J**-freezing line, a FL-to-NFL crossover appears with a peculiar flavor selectivity in the NFL phase. This is a unique feature of SOC, which is not present in models with ordinary crystal-field splitting. We expect that hole-doping of materials with d^5 filling like iridates or rhodates will shift the systems toward the **J**-freezing line. Near $n = 4$, we observe excitonic magnetism with both AFM and FM order that is consistent with a recent mean-field study [8]. Upon electron doping, the AFM state at $n = 4$ is suppressed and the FM state emerges with enhanced Hund's coupling. These results offer new routes for finding exotic phases by doping $4d$ and $5d$ based materials.

We thank Ying Li, Steffen Backes, Steve Winter, Ryui Kaneko, Jan Kuneš, Alexander I. Lichtenstein, Jeroen van den Brink, Bernd Büchner, Laura Teresa Corredor Bohorquez, and Gang Cao for helpful discussions. This research was supported by the German Research Foundation (Deutsche Forschungsgemeinschaft) through Grant No. FOR 1346. The computations were performed at the Center for Scientific Computing (CSC), Goethe-Universität Frankfurt.

*aaram@itp.uni-frankfurt.de

[1] B. J. Kim, H. Ohsumi, T. Komesu, S. Sakai, T. Morita, H. Takagi, and T. Arima, Phase-sensitive observation of a spin-orbital Mott state in Sr_2IrO_4, Science **323**, 1329 (2009).

[2] J. Chaloupka, G. Jackeli, and G. Khaliullin, Kitaev-Heisenberg Model on a Honeycomb Lattice: Possible Exotic Phases in Iridium Oxides A_2IrO_3, Phys. Rev. Lett. **105**, 027204 (2010).

[3] R. Comin G. Levy, B. Ludbrook, Z.-H. Zhu, C. N. Veenstra, J. A. Rosen, Yogesh Singh, P. Gegenwart, D. Stricker, J. N. Hancock, D. van der Marel, I. S. Elfimov, and A. Damascelli, Na_2IrO_3 as a Novel Relativistic Mott Insulator with a 340-meV Gap, Phys. Rev. Lett. **109**, 266406 (2012).

[4] K. W. Plumb, J. P. Clancy, L. J. Sandilands, V. V. Shankar, Y. F. Hu, K. S. Burch, H.-Y. Kee, and Y.-J. Kim, α- RuCl3: A spin-orbit assisted Mott insulator on a honeycomb lattice, Phys. Rev. B **90**, 041112 (2014).

[5] S. M. Winter, Y. Li, H. O. Jeschke, and R. Valentí, Challenges in design of Kitaev materials: Magnetic interactions from competing energy scales, Phys. Rev. B **93**, 214431 (2016).

[6] F. Lang, P. J. Baker, A. A. Haghighirad, Y. Li, D. Prabhakaran, R. Valentí, and S. J. Blundell, Unconventional magnetism on a honeycomb lattice in $\alpha - RuCl_3$ studied by muon spin rotation, Phys. Rev. B **94**, 020407 (2016).

[7] Z. Y. Meng, Y. B. Kim, and H.-Y. Kee, Odd-Parity Triplet Superconducting Phase in Multiorbital Materials with a Strong Spin-Orbit Coupling: Application to Doped Sr_2IrO_4, Phys. Rev. Lett. **113**, 177003 (2014).

[8] J. Chaloupka and G. Khaliullin, Doping-Induced Ferromagnetism and Possible Triplet Pairing in d^4 Mott Insulators, Phys. Rev. Lett. **116**, 017203 (2016).

[9] W. Witczak-Krempa, G. Chen, Y. B. Kim, and L. Balents, Correlated quantum phenomena in the strong spin-orbit regime, Annu. Rev. Condens. Matter Phys. **5**, 57 (2014).

[10] G. Khaliullin, Excitonic magnetism in Van Vleck-Type d^4 Mott Insulators, Phys. Rev. Lett. **111**, 197201 (2013).

[11] O. N. Meetei, W. S. Cole, M. Randeria, and N. Trivedi, Novel magnetic state in d^4 Mott insulators, Phys. Rev. B **91**, 054412 (2015).

[12] G. Chen and L. Balents, Spin-orbit coupling in d^2 ordered double perovskites, Phys. Rev. B **84**, 094420 (2011).

[13] G. Chen, R. Pereira, and L. Balents, Exotic phases induced by strong spin-orbit coupling in ordered double perovskites, Phys. Rev. B **82**, 174440 (2010).

[14] O. N. Meetei, O. Erten, M. Randeria, N. Trivedi, and P. Woodward, Theory of High T_c Ferrimagnetism in a Multi-orbital Mott Insulator, Phys. Rev. Lett. **110**, 087203 (2013).

[15] Y. Singh and P. Gegenwart, Antiferromagnetic Mott insulating state in single crystals of the honeycomb lattice material Na_2IrO_3, Phys. Rev. B **82**, 064412 (2010).

[16] R. D. Johnson, S. C. Williams, A. A. Haghighirad, J. Singleton, V. Zapf, P. Manuel, I. I. Mazin, Y. Li, H. O. Jeschke, R. Valentí, and R. Coldea, Monoclinic crystal structure of $\alpha - RuCl_3$ and the zigzag antiferromagnetic ground state, Phys. Rev. B **92**, 235119 (2015).

[17] H. Shinaoka, S. Hoshino, M. Troyer, and P. Werner, Phase Diagram of Pyrochlore Iridates: All-in–all-out Magnetic Ordering and Non-Fermi-Liquid Properties, Phys. Rev. Lett. **115**, 156401 (2015).

[18] K. Foyevtsova, H. O. Jeschke, I. I. Mazin, D. I. Khomskii, and R. Valentí, *Ab initio* analysis of the tight-binding parameters and magnetic interactions in Na_2IrO_3, Phys. Rev. B **88**, 035107 (2013).

[19] J. Kanamori, Electron correlation and ferromagnetism of transition metals, Prog. Theor. Phys. **30**, 275 (1963).

[20] A. Georges, G. Kotliar, W. Krauth, and M. J. Rozenberg, Dynamical mean-field theory of strongly correlated fermion systems and the limit of infinite dimensions, Rev. Mod. Phys. **68**, 13 (1996).

[21] E. Gull, A. J. Millis, A. I. Lichtenstein, A. N. Rubtsov, M. Troyer, and P. Werner, Continuous-time Monte Carlo methods for quantum impurity models, Rev. Mod. Phys. **83**, 349 (2011).

[22] P. Werner and A. J. Millis, Hybridization expansion impurity solver: General formulation and application to Kondo lattice and two-orbital models, Phys. Rev. B **74**, 155107 (2006).

[23] T. Sato, T. Shirakawa, and S. Yunoki, Spin-orbit-induced exotic insulators in a three-orbital Hubbard model with $(t_{2g})^5$ electrons, Phys. Rev. B **91**, 125122 (2015).

[24] S. Hoshino and P. Werner, Superconductivity from Emerging Magnetic Moments, Phys. Rev. Lett. **115**, 247001 (2015).

[25] See Supplemental Material at http://link.aps.org/supplemental/10.1103/PhysRevLett.118.086401, which includes Refs. [26–31], for data of the **J**-correlation function and local susceptibility, the analysis of the local Hamiltonian and the magnetic phases, and the summary of the reported parameter values for various materials.

[26] M. W. Haverkort, I. S. Elfimov, L. H. Tjeng, G. A. Sawatzky, and A. Damascelli, Strong Spin-Orbit Coupling Effects on the Fermi Surface of Sr_2RuO_4 and Sr_2RhO_4, Phys. Rev. Lett. **101**, 026406 (2008).

[27] L. Vaugier, H. Jiang, and S. Biermann, Hubbard U and Hund exchange J in transition metal oxides: Screening versus localization trends from constrained random phase approximation, Phys. Rev. B **86**, 165105 (2012).

[28] I. I. Mazin and D. J. Singh, Electronic structure and magnetism in Ru-based perovskites, Phys. Rev. B **56**, 2556 (1997).

[29] K. Pajskr, P. Novák, V. Pokorný, J. Kolorenč, R. Arita, and J. Kuneš, On the possibility of excitonic magnetism in Ir double perovskites, Phys. Rev. B **93**, 035129 (2016).

[30] S. Gangopadhyay and W. E. Pickett, Interplay between spin-orbit coupling and strong correlation effects: Comparison of the three osmate double perovskites Ba_2AOsO_6 (A = Na, Ca, Y), Phys. Rev. B **93**, 155126 (2016).

[31] K.-W. Lee and W. E. Pickett, Orbital-quenching-induced magnetism in Ba_2NaOsO_6, Europhys. Lett. **80**, 37008 (2007).

[32] H. Watanabe and T. Shirakawa, and S. Yunoki, Microscopic Study of a Spin-Orbit-Induced Mott Insulator in Ir Oxides, Phys. Rev. Lett. **105**, 216410 (2010).

[33] P. Werner, E. Gull, M. Troyer, and A. J. Millis, Spin Freezing Transition and Non-Fermi-Liquid Self-Energy in a Three-Orbital Model, Phys. Rev. Lett. **101**, 166405 (2008).

[34] L. de' Medici, J. Mravlje, and A. Georges, Janus-Faced Influence of Hund's Rule Coupling in Strongly Correlated Materials, Phys. Rev. Lett. **107**, 256401 (2011).

[35] L. Du, L. Huang, and X. Dai, Metal-insulator transition in three-band Hubbard model with strong spin-orbit interaction, Eur. Phys. J. B **86**, 94 (2013).

[36] J. Bünemann, T. Linneweber, U. Löw, F. B. Anders, and F. Gebhard, Interplay of Coulomb interaction and spin-orbit coupling, Phys. Rev. B **94**, 035116 (2016).

[37] N. Ashcroft and N. Mermin, *Solid State Physics* (Saunders College, Philadelphia, 1976).

[38] L. de' Medici, S. R. Hassan, M. Capone, and X. Dai, Orbital-Selective Mott Transition Out of Band Degeneracy Lifting, Phys. Rev. Lett. **102**, 126401 (2009).

[39] J. Kuneš, Phase diagram of exciton condensate in doped two-band Hubbard model, Phys. Rev. B **90**, 235140 (2014).

[40] H. Zhang, J. Terizc, F. Ye, P. Schlottmann, H. D. Zhao, S. J. Yuan, and G. Cao, Breakdown of the spin-orbit imposed $J_{\mathrm{eff}} = 0$ singlet state in double-perovskite iridates with $Ir^{5+}(5d^4)$ ions, arXiv:1608.07624.

[41] T. Sato, T. Shirakawa, and S. Yunoki, Spin-orbital entangled excitonic insulators in $(t_{2g})^4$ correlated electron systems, arXiv:1603.01800v1.

[42] S. Hoshino and P. Werner, Electronic orders in multiorbital Hubbard models with lifted orbital degeneracy, Phys. Rev. B **93**, 155161 (2016).

[43] L. T. Corredor, G. Aslan-Cansever, M. Sturza, K. Manna, A. Maljuk, S. Gass, A. Zimmermann, T. Dey, C. G. F. Blum, M. Geyer, A. U. B. Wolter, S. Wurmehl, and B. Buechner, The iridium double perovskite Sr_2YIrO_6 revisited: A combined structural and specific heat study, arXiv:1606.05104 [Phys. Rev. B (to be published)].

[44] T. Dey, A. Maljuk, D. V. Efremov, O. Kataeva, S. Gass, C. G. F. Blum, F. Steckel, D. Gruner, T. Ritschel, A. U. B. Wolter, J. Geck, C. Hess, K. Koepernik, J. van den J. Brink, S. Wurmehl, and B. Büchner, Ba_2YIrO_6: A cubic double perovskite material with Ir^{5+} ions, Phys. Rev. B **93**, 014434 (2016).